Multiple Scattering by NMR

Yuan Cheng† and David G. Cory*

Department of Nuclear Engineering
Massachusetts Institute of Technology
NW14-4111, 150 Albany Street
Cambridge, Massachusetts 02139
Received December 15, 1998
Revised Manuscript Received June 2, 1999

NMR scattering experiments are widely used to explore structure at the μm scale in samples with boundaries to molecular diffusion,[1] such as biological samples, food, geologic sediments, and industrial materials. Typical questions include the distribution of pore sizes, the interconnections, the surface to volume ratio, and the 3-D geometry of individual pores. Here, for the first time, multiple scattering by NMR is demonstrated. In particular, these experiments can quantify the eccentricities and symmetries of confining cavities, even with no bulk order in the sample. The experimental setup, method, and theory are introduced, along with measurements on yeast cells that have varied cell eccentricities.

The difference between NMR imaging and scattering measurements lies in the information carried by the phase of the nuclear spin magnetization. In imaging, the phase labels the position of each spin, while in scattering, the phase labels the displacement of the spin over a short interval (milliseconds to seconds). In imaging, a Fourier transform of the signal returns the location of each spin (an image), while in scattering, a Fourier analysis returns the distribution of spin displacements but has no information about the absolute location of any spin.

The simplest NMR scattering experiment, the pulsed gradient spin echo (PGSE) method, was introduced by Stejskal to study molecular diffusion.[3] It was pointed out that the analysis of diffusion data could be performed in Fourier space, yet the scattering analogy was not stressed until comparisons with incoherent thermal neutron scattering were made.[4] There have been proposals to extend the NMR diffusion measurement to multiple events.[6,7] Here we report the first description of an actual experiment and its results.

Neutron and X-ray scattering focus on single scattering events since the scattering vectors cannot be controlled. In NMR scattering, the scattering vector is determined by the direction, amplitude, and duration of magnetic gradient pulses and hence is controlled. This makes NMR multiple scattering little more difficult than NMR single scattering. The advantage offered by NMR multiple scattering is that, when the angle between the scattering vectors is changed from parallel to perpendicular, the experiment probes the 2-D cross-sectional area of the sample.

A scattering measurement depends on spin evolution in a magnetic field gradient ($\nabla_u B_z$, where $u = x, y, z$) so as to spatially label the spin's phase by its location in the gradient field

$$\text{phase} = \gamma \nabla B_z \cdot \mathbf{r} t \tag{1}$$

This linear phase ramp corresponds to a spin magnetization helix with a wave number, $\mathbf{q} = \gamma \nabla B_z t$.

In the PGSE experiment, shown in Figure 1, the gradient pulse

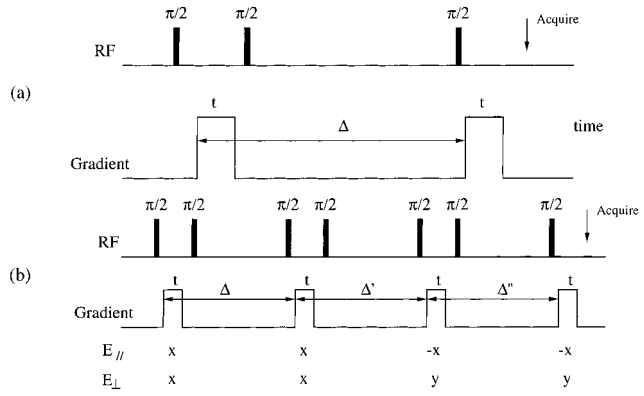

Figure 1. (a) Single event NMR scattering experiment: the pulsed gradient stimulated echo (PGSTE) experiment. (b) Double event NMR scattering experiments with scattering vectors parallel or perpendicular.

winds the spin magnetization into a spatial helix $e^{i\mathbf{q}\cdot\mathbf{r}}$. The spins now move according to a conditional displacement probability $P(\mathbf{r}|\mathbf{r}', t)$, the probability that the particle starting at position $\mathbf{r}$ will be at $\mathbf{r}'$ at time t. The spatial magnetization grating is blurred by the random motions of the spins and the scattering measurement is the phase/amplitude of the residual grating. This residual grating is made observable by an inverse magnetic field gradient pulse $-\nabla B_z$, which unwinds the magnetization grating and changes the phase labeling to spatial displacements rather than positions. The total average phase change $\langle e^{i\mathbf{q}\cdot(\mathbf{r}-\mathbf{r}')}\rangle$, is proportional to the NMR signal induced in a homogeneous RF coil, yielding the net signal integrated over the whole sample

$$E(q, \Delta) = E(0, \Delta)\langle e^{i\mathbf{q}\cdot(\mathbf{r}-\mathbf{r}')}\rangle = \int_V \rho(\mathbf{r}) P(\mathbf{r}|\mathbf{r}', \Delta) e^{i\mathbf{q}\cdot(\mathbf{r}-\mathbf{r}')} d^3\mathbf{r} d^3\mathbf{r}' \tag{2}$$

where $\rho(\mathbf{r})$ is the normalized local spin density function and $E(0, \Delta)$ is the signal when $q = 0$.

If the molecules are fully bounded within each pore, then the sample can be expressed as

$$\rho(\mathbf{r}) = \sum_i \eta_i(\mathbf{r}) \tag{3}$$

where η's are the shape function of the pores. Cory and Garroway showed that, as $\Delta \rightarrow \infty$, the scattering signal is the autocorrelation of the projection of the sample structure along the gradient direction, with a correlation length equal to the pore diameter.[8] The physical significance of the autocorrelation is that the spins were free to sample all locations within a pore.

In this fully bounded and δ-function gradient pulse limit, $P(\mathbf{r}|\mathbf{r}', t)$ can be approximated by the shape function $\eta_i(\mathbf{r}')$ of the i'th pore confining the molecule. The signal is then,

$$E(q, \infty) = \sum_i^{\text{all pores}} \int \eta_i(\mathbf{r}') e^{i\mathbf{q}\cdot(\mathbf{r}-\mathbf{r}')} d^3\mathbf{r}' \tag{4}$$

rewritten following the Wiener Kintchin theorem in real space as

$$\tilde{E}(u) = \sum_i \tilde{\eta}_i(u) \odot \tilde{\eta}_i(u) \tag{5}$$

where $\tilde{\eta}$'s are the Fourier counterparts of the pore shape functions.

* Author to whom correspondence should be addressed.
† Current address: GE Corporate Research and Development, K1-NMR-137, 1 Research Circle, Schenectady, NY 12309.

(1) Callaghan, P. T. *Principles of NMR Microscopy*; Oxford, 1991.
(2) Mansfield, P.; Grannel, P. K. *J. Phys. C* **1973**, *6*, L422.
(3) Stejskal, E. O.; Tanner, J. E. *J. Chem. Phys.* **1965**, *42*, 288.
(4) Fleischer, G.; Fujara, F. *NMR Basic Principles and Progress* **1994**, *30*, 159.
(5) Callaghan, P. T.; Coy, A.; MacGowan, D.; Parker, K. J.; Zelaya, F. O. *Nature* **1991**, *351*, 467.
(6) Cory, D. G.; Garroway, A. N.; Miller, J. B. *Polym. Prep.* **1990**, *31*, 149.
(7) Mitra, P. P., personal communication, 1994.
(8) Cory, D. G.; Garroway, A. *Magn. Reson. Med.* **1990**, *14*, 435.

10.1021/ja9843324 CCC: $18.00
Published on Web 08/14/1999

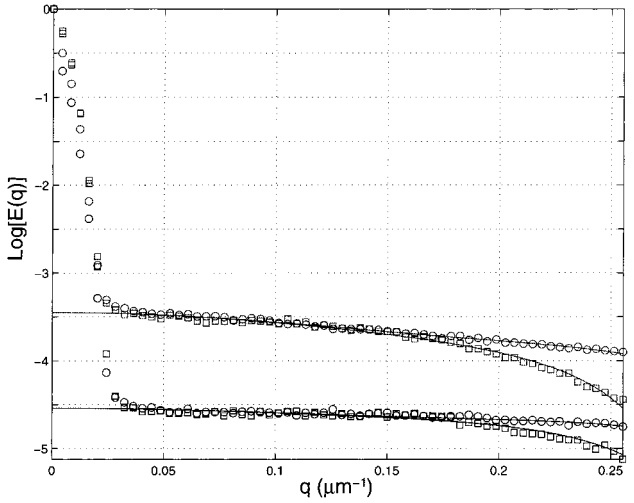

Figure 2. Double event scattering curves for medium-long yeast cells (upper pair) and extra-long yeast cells (lower pair). The open circles and squares correspond to scattering of parallel and perpendicular scattering vectors, respectively. The solid lines are fitted to a power series with seven terms. For both data sets the maximum gradient strength was 600 G/cm, the gradient pulse length was 1.0 ms, and the mixing times were 20 ms. The time between the two scattering events was 40 ms.

The single scattering measurement is a weighted average of the displacement profiles along a single laboratory frame direction; therefore, if the sample consists of a simple pore shape repeated with random orientations, the overall scattering curve reflects this powder distribution. However, there is insufficient information for the scattering signal to the inverted to the pore shape function. Without a model based on prior knowledge, the distribution of orientation can not be separated from a distribution of sizes in this simple experiment.

The NMR double scattering experiment is an extension of the PGSE experiment, see Figure 1B. At time Δ' after the first scattering event, a second magnetization grating is created, either along the same direction as the first, $e^{iq_x x''}$, or along a perpendicular direction, $e^{iq_y y}$, and with the same amplitude of wave number. The system is now allowed to diffuse for a time Δ'', and thus the molecular displacements within the two diffusion time intervals are correlated. The echo attenuation for the parallel, $E_{||}(q)$, and perpendicular case, $E_{\perp}(q)$, are

$$E_{||}(q) = \int \rho(\mathbf{r})P(\mathbf{r}|\mathbf{r}', \Delta)e^{i\mathbf{q}\cdot(\mathbf{r}-\mathbf{r}')} \times P(\mathbf{r}'|\mathbf{r}'', \Delta')P(\mathbf{r}''|\mathbf{r}''', \Delta'')e^{i\mathbf{q}\cdot(\mathbf{r}''-\mathbf{r}'')}\, d^3\mathbf{r}d^3\mathbf{r}'d^3\mathbf{r}''d^3\mathbf{r}''' \quad (6)$$

$$E_{\perp}(q) = \int \rho(\mathbf{r})P(\mathbf{r}|\mathbf{r}', \Delta)e^{i\mathbf{q}\cdot(\mathbf{r}-\mathbf{r}')} \times P(\mathbf{r}'|\mathbf{r}'', \Delta'')P(\mathbf{r}''|\mathbf{r}'', \Delta'')e^{i\mathbf{q}_{\perp}\cdot(\mathbf{r}''-\mathbf{r}'')}d^3\mathbf{r}d^3\mathbf{r}'d^3\mathbf{r}''d^3\mathbf{r}''' \quad (7)$$

Notice that these are 1-D NMR measurements of double scattering events. The correlations for the parallel and perpendicular cases reflect the restricting geometries along the two directions. By comparing these two signals, the anisotropy of diffusion can be directly characterized.

A simple and useful model of a confining geometry is a set of randomly oriented ellipsoids. The Supporting Information shows and analytic derivation of multiple scattering curves as well as plots of $E_{||}$ and $E_{\perp}$.

The experiments were run on a Bruker AMX-600 NMR spectrometer with a home-built microscopy probe that provides gradient fields of up to 1250 G/cm. The samples were normal round yeast cells and radiation treated yeast cells whose DNA had lost its ability to duplicate. When the treated cells fail to divide, they became pronouncedly prolate. The eccentricities of the prolate cells were controlled by the culture times. Light microscope pictures of the cells are shown in the Supporting Information. The two groups of prolate cells have ratios of the minor to major axes of approximately $^1/_5$ and $^1/_{10}$. The cells were placed in 1-mm diameter capillary tubes and mildly centrifuged for 1 min.

The double scattering experiments on cells with different eccentricities are shown in Figure 2. Notice that the scattering curves of $E_{||}$ are higher than those of $E_{\perp}$, and for cells with larger eccentricities the slope falls faster with q, consistent with the calculations. The initial decay at low q is from extracellular water. Also notice that the curves for the extra-long cells yield larger splittings than that of medium-long cells.

To measure the average pore eccentricity from the two scattering curves, a moment analysis is convenient. The power expansion of the scattering function for ellipsoids with semi-major radii of a and b, up to the fourth power are

$$E_{||}(q) = 1 + c_2q^2 + c_4q^4 \quad (8)$$

$$E_{\perp}(q) = 1 + d_2q^2 + d_4q^4 \quad (9)$$

where

$$c_2 = d_2 = -\frac{2}{5}\left(\frac{2}{3}a^2 + \frac{1}{3}b^2\right) \quad (10)$$

$$c_4 - d_4 = \frac{2}{375}(a^2 - b^2)^2 \quad (11)$$

The eccentricities follow these equations. The coefficients of the moment analysis are obtained by extrapolating the fitted curves of the experimental data towards the origin. For the medium and long cells, c_2 are -5.95 and -12.2, respectively, $c_4 - d_4$ are 9 and 41.3, respectively. The calculated average end-to-end sizes for the two prolate yeast cells are 2.18/2.18/13.0 (μm) and 2.16/2.16/18.88 (μm). While these numbers are in reasonable agreement with the microscopy results, it must be remembered that the spins are confined to the interior of the cells and diffusion during gradient pulses tends to reduce the measured dimension.[9] This can be compensated for in a more complicated analysis.

The shape of the cells, either prolate or oblate, is determined by the sign of $\sqrt{c_4 - d_4}$ which decides if a or b is the long semiradius. Since, in the above analysis, the axis system is always chosen to be around b, $b < a$ corresponds to oblate shapes.

The microscopic directional correlation of multiple scattering events is a unique feature of NMR scattering and a potentially powerful means of exploring pore shapes. In particular it permits the separation of pore shapes from distributions of pore orientations. The spatial and temporal region of NMR scattering is determined by the diffusion coefficient and longitudinal relaxation time. These two scattering regions are extended in NMR (seconds in temporal and μms in spatial resolution). It typically permits spatial measurements from $0.2 \rightarrow 25$ μm.

Acknowledgment. The authors thank Mr. Cory Kostrub from the Genetics Laboratory of Harvard Medical School for providing the long yeast cells and Dr. Yan Shao from the materials science group at the DEAS of Harvard University for taking the light microscopic pictures.

Supporting Information Available: Analytic derivation of multiple scattering curves and plots of $E_{||}$ and $E_{\perp}$ (PDF). This material is available free of charge via the Internet at http://pubs.acs.org.

JA9843324

(9) Mitra, P. P.; Halperin, B. I. *J. Magn. Reson. A* **1995**, *113*, 94.